## POLITECNICO DI TORINO Repository ISTITUZIONALE

#### 3D-printed wideband reflectarray antennas with mechanical beam-steering

#### Original

3D-printed wideband reflectarray antennas with mechanical beam-steering / Massaccesi, Andrea; Beccaria, Michele; Bertana, Valentina; Marasso, Simone Luigi; Cocuzza, Matteo; Dassano, Gianluca; Pirinoli, Paola. - In: INTERNATIONAL JOURNAL OF MICROWAVE AND WIRELESS TECHNOLOGIES. - ISSN 1759-0787. - ELETTRONICO. - 16:(2024), pp. 21-29. [10.1017/s1759078723000776]

Availability:

This version is available at: 11583/2992557 since: 2024-10-21T11:46:41Z

Publisher:

Cambridge University Press

Published

DOI:10.1017/s1759078723000776

Terms of use:

This article is made available under terms and conditions as specified in the corresponding bibliographic description in the repository

Publisher copyright

Cambridge University Press postprint/Author's Accepted Manuscript

This article has been published in a revised form in INTERNATIONAL JOURNAL OF MICROWAVE AND WIRELESS TECHNOLOGIES http://doi.org/10.1017/s1759078723000776. This version is free to view and download for private research and study only. Not for re-distribution or re-use. © copyright holder.

(Article begins on next page)

# **3D-printed Wideband Reflectarray Antennas** with Mechanical Beam-Steering

andrea massaccesi $^1$ , michele beccaria $^1$ , valentina bertana $^{2,3}$ , simone luigi marasso $^{2,3,4}$ , matteo cocuzza $^{2,3,4}$ , gianluca dassano $^1$  and paola pirinoli $^{1,5}$ 

This paper investigates the performance of 3D-printed dielectric reflectarray antennas with wideband behavior and beam-steering capabilities. The designed unit-cell consists of a single-layer dielectric element perforated with a square hole, whose side is used to control the local variation of the reflection coefficient. The numerical analysis of the unit-cell and a of first  $52 \times 52$  reflectarray working in Ka-band, whose scanning capabilities are tested just moving the feed along an arc, confirms that the unit-cell has a stable behaviour with respect to both the frequency and the direction of arrival of the incident field. In view of these promising capabilities, the proposed unit-cell is used to design a bifocal reflectarray with the same size and working in the same frequency band of the first one. Its numerical characterization and the measurements of a prototype prove that the RA is able to provide less than  $0.8\,\mathrm{dB}$  of gain losses over a scanning range of  $\pm 40^\circ$  in the vertical plane, while the bandwidth varies between 13.5% and 28%, depending on the pointing direction. The obtained results demonstrate the effectivness of the proposed approach and highlight the potential of 3D-printing technology for producing high-performance, cost-effective reflectarray antennas with wideband behavior and excellent beam-steering features.

Keywords: Reflectarray antennas, periodic structures, perforated dielectric, 3D-printing, additive manufacturing.

#### I. INTRODUCTION

Next generation antennas will need to be characterized by a wideband behaviour and by reconfigurability to generate multiple or scanning beams. To achieve these aims, several options have been proposed, and among them the possibility to use Reflectarray Antennas (RAs) [1, 2] has also been considered. Despite of their copious advantages, RAs present also some drawbacks, the principal of which is a reduced bandwidth, essentially due to the intrinsic narrow bandwidth of single layer printed elements, widely used for the realization of the RA Unit-Cells (UCs), and to the frequency dependence of the path from the feed to the different points on the planar surface. To overcome this limitation the use of elements with more degrees of freedom, printed on different layers, as in [3, 4] or on the same dielectric substrate [5]-[9], were introduced. Recently, the design of dielectric-only RAs is becoming popular, especially at mm-waves and sub-THz frequencies, where the metal losses are significant. Among the other potentialities, dielectriconly structures present a wider bandwidth and a low manufacturing cost that makes feasible the manufacturing of reradiating elements with arbitrary shapes. On the other hand, they are also responsible of some restrictions, related to the available materials, in most of the cases characterized by a low value of the relative dielectric constant and by high losses, to the printer resolution, that affects the minimum realizable size, and to the size of the printing plate.

Several examples of 3D-printed dielectric-only reflectarrays are available in literature. The configurations proposed in [10, 11] use dielectric parallelepiped resonators as unit-cells, whose height is varied to control the phase of the reradiated field. The 3D-printed prototype in [10] has an aperture of  $12\lambda \times 12\lambda$  and shows a 1-dB bandwidth of almost 10%, while that in [11] is characterized by a size of  $20.5\lambda \times 20.5\lambda$  at sub-THz frequencies and 1-dB bandwidth slightly lower than 21%. The configuration in [12] uses hemi-ellipsoidal dielectric resonators as reradiating elements: the designed antenna has an aperture size of  $5.5\lambda \times 5.5\lambda$  and 1-dB bandwidth of 11.2%. In [13] a C-shaped dielectric unit-cell with height approximately equal to  $1.5\lambda$  is adopted for the design of a center fed RA with diameter of  $10\lambda$ . The 1-dB bandwidth in the case in which the radiated field is linearly polarized is slightly smaller than 12%. The reflectarray in [14] has an aperture of  $11.2\lambda \times 11.2\lambda$ , discretized with cross-shape elements and provides a

**Corresponding author:** Andrea Massaccesi Email: andrea.massaccesi@polito.it

<sup>&</sup>lt;sup>1</sup>Department of Electronics and Telecommunications, Politecnico di Torino, 10129 Torino, Italy

<sup>&</sup>lt;sup>2</sup>Department of Applied Sciences and Technology, Politecnico di Torino, 10129 Torino, Italy

<sup>&</sup>lt;sup>3</sup>Chilab-Materials and Microsystems Laboratory, 10034 Chivasso (TO), Italy

<sup>&</sup>lt;sup>4</sup>IMEM-CNR, 43124 Parma, Italy

<sup>&</sup>lt;sup>5</sup>IEIIT-CNR, 10129 Torino, Italy

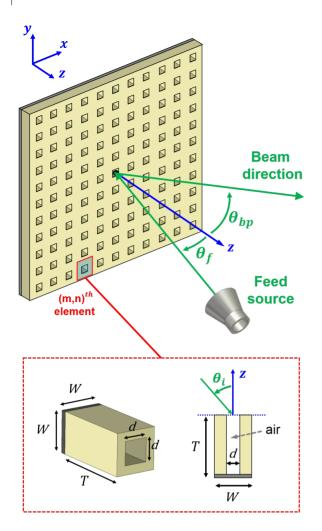


Fig. 1.: Sketch of the antenna configuration with the unit-cell in the inset.

1-dB bandwidth of 10.7%, while in [15] a Kirigami inspired two stage snapping-like element is introduced for the realization of a  $11.37\lambda \times 11.37\lambda$  RA with a 1-dB bandwidth of 16.3%. Finally, the solution in [16] adopts two orthogonal dielectric cuboids to design a  $10.7\lambda \times 10.7\lambda$  aperture able to generate a dual circularly polarized field over a 1-dB bandwidth  $\approx 13\%$ .

For what concerns the multi or scanning beam capability, the most straightforward solution is to design a reflectarray in which the behaviour of the unit-cell is controlled through active elements as pin diodes [17]-[22], varactors, [23]-[26], MEMS switches [27] or using for its realization liquid crystal [28]-[30] or liquid metal [31]. All these choices strongly affect the complexity and the cost of the antenna and therefore possible alternatives have been studied. If few projects, as the one in [32], are aimed to reduced the control points in the active reflecting surface, in other configurations the RA is passive and the beam-steering is obtained by mechanically rolling the aperture [33] or more commonly moving

mechanically the feed or using a feed array to change the direction of arrival of the field impinging on the reflecting surface [34]-[36].

Despite of its greater simplicity, such an antenna suffers for some degradations of its radiation performance, as the enlargement of the main beam, an increase in the side-lobe level (SLL), a lowering of the maximum gain, that further decreases over the scan range, a narrowing of the bandwidth. To improve the RA features, different techniques have been proposed, as that of designing a bifocal [37, 38] or a multifocal [39] reflectarray; in [40] the RA is designed to behave as a quasi-spherical reflector, while in [41] the planar reflector is rotated in addition to the feed to cover a larger scan range. Finally, the results summarized in [37, 42] prove that a pseudo-stochastic optimization algorithm can be fruitfully adopted to design a beam-scanning reflectarray with enhanced performance.

As for the bandwidth, the reflectarray beam-scanning capabilities also depend on the properties of the unit-cell. In fact, its behaviour is affected by the direction of arrival of the incident field and hence when it changes the UC generally does not provide the required phase compensation and this results in a degradation of the antenna radiation properties. To reduce this effect it is therefore useful to adopt a proper unit-cell in addition to a suitable design procedure.

In this context, the possibility of using a unit-cell alike the one introduced in [43] for the realization of a beam-steering RA, is investigated. Some preliminary numerical results on the scanning beam behaviour of a RA consisting of  $52 \times 52$  are already collected in [44], but the unit-cell adopted there, as the one in [43], does not fulfil the constrains imposed by the Additive Manufacturing (AM) technique selected for the antenna realization even if the results in [43, 44] confirm that the UC posses the proper features for its use in the design of a scanning beam reflectarray with enhanced bandwidth. Here, the limitations introduced by the AM are taken into account and a printable version of the unit-cell is defined, as it is described in Sect.II. To verify its features and in particular its dependence from the angle of incidence, a first, single focus RA is designed, and then its beamsteering capability is checked rotating the feed along an arc. In view of the encouraging numerical results summarized in Sect.III.A, a bifocal RA is finally designed and manufactured. The numerical analysis and the experimental characterization of the prototype reported in Sect.III.B show that the gain scan losses are lower than 0.8 dB over a scanning range of  $\pm 40^{\circ}$ , while the bandwidth varies between 13.5% and 28% over this interval.

#### II. DIELECTRIC UNIT-CELL

The adopted unit-cell is an optimized version of those introduced in [43, 44]. As shown in the inset of Fig. 1, it consists in a dielectric parallelepiped with square basis, backed on a metallic ground plane, and having a square hole in the center, whose side d is varied to control the reflection coefficient  $S_{11}$ , while its height T is kept constant. The change of the hole size corresponds to modify the ratio between the quantity of dielectric material and air in the unit-cell, resulting in a variation of its effective dielectric constant.

To make possible the printing of the unit-cell with an AM technique, and in particular with a PolyJet printer, a suitable dielectric material must be used. Here, the chosen material is the 3D-printable resin VeroWhitePlus<sup>TM</sup> provided by Stratasys<sup>®</sup> and characterized by  $\varepsilon_r=2.77$  and  $\tan\delta=0.021$ , which is the same used in [45, 46]. The unit-cell has been designed in Ka-band at the operating frequency  $f_0 =$ 30 GHz. Since the structures proposed in [43, 44] were not suitable for 3D printing, a new version of the unit-cell was optimized to maximize its performance while taking into account the limitations of the additive manufacturing process. To determine the appropriate geometrical parameters for the unit-cell that would allow for its fabrication, several test samples of dielectric sheets with square holes of varying sizes and heights were printed. After a thorough analysis, it was found that for small holes, the actual value of d was significantly smaller, and there was an increased risk of unwanted polymerization of small resin residues that could clog up the hole. In order to solve these issues, it was determined that the height of the unit-cell should be maintained at a minimum of 6 mm, and the size of the holes d should be varied within the range [0.8, 2.55] mm. This strategy aims to prevent systematic printing errors and to ensure that the holes are as accurate as possible. The optimal geometric parameters for the unitcell, that satisfy the aforementioned requirements and maximize the performance, are the following: W = $0.3\lambda_0 = 3 \,\mathrm{mm}$ , being  $\lambda_0$  the wavelength evaluated at  $f_0$ ,  $T = 0.8\lambda_0 = 8$  mm while d can vary between 0.8 mm and 2.55 mm. They are obtained following an optimization process organized in the three steps listed below.

- 1) Choice of the size W of the unit-cell: a smaller value guarantees a better sampling of the aperture and improves the antenna bandwidth, but reduces the possible range of variation for the hole size d.
- 2) Determination of the range of variation of the hole size d: if it is larger the range of variation for the phase of the reflection coefficient is wider, but either too small or too large values for d must be

- avoided since they correspond to a unit-cell that cannot be manufactured.
- 3) Selection of T: increasing the height of the UC it is possible to enlarge the range of variation for the phase of  $S_{11}$ , but at the cost of a worsening of the losses introduced by the material and of a more bulky structure.

In Fig. 2 it is plotted the frequency behaviour of the amplitude (top) and phase (bottom) of the reflection coefficient, for different values of the hole size. It can be noticed that the phase varies linearly over the entire frequency range, and that its behaviour is almost the same for all the considered values of d, as proved by the fact that the different lines are almost parallel; the amplitude of  $S_{11}$  is never lower than -1.5 dB when  $d \geq 2$  mm, while its value decreases for smaller holes, due to the increase of losses. The dependence of the reflection coefficient from frequency, and in particular

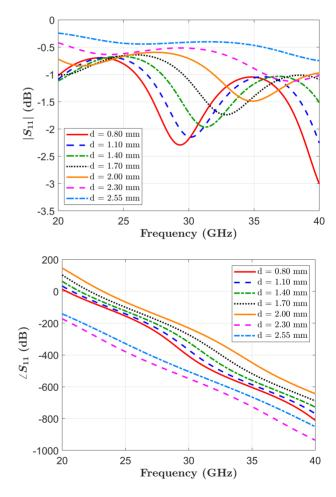


Fig. 2.: Unit-cell: Variation of the simulated reflection coefficient  $S_{11}$  with the frequency for different values of d. Top: amplitude. Bottom: phase. (UC dimensions:  $W=3 \, \mathrm{mm}$ ,  $T=0.8 \, \mathrm{mm}$ ,  $d=[0.8 \, , 2.55] \, \mathrm{mm}$ )

the linear behaviour of the phase, confirm the wide band aptitude of the unit-cell.

Since the UC would be used for the design of a beam-steering RA, its dependence from the direction of arrival of the incident field is also studied. In Fig. 3 it is plotted the variation of the amplitude (top) and phase (bottom) of  $S_{11}$  with the angle of incidence  $\theta_i$ , evaluated for different values of d at the design frequency  $f_0$ . As can be seen from these results,  $\angle S_{11}$ does not change significantly till  $\theta_i = 40^\circ$ , while the amplitude of the reflection coefficient behaves in a different way depending on the hole size. In particular, when it is small,  $|S_{11}|$  reaches values even below -2.5 dB for  $\theta_i \approx 30^{\circ}$ . For larger d, the influence of the direction of arrival of the incident field is negligible, and this confirms the possibility to use the considered unit-cell for the design of a beam-steering reflectarray.

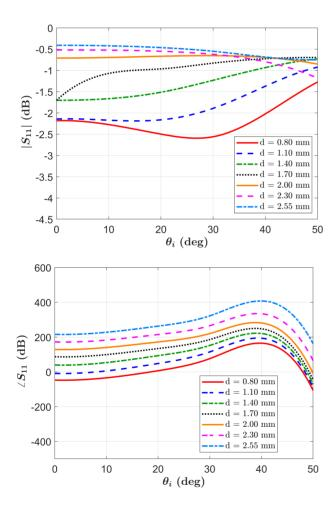


Fig. 3.: Unit-cell: Variation of the simulated reflection coefficient  $S_{11}$  with the angle of incidence  $\theta_i$  at 30 GHz for different values of d. Top: amplitude. Bottom: phase. (UC dimensions: W=3 mm, T=0.8 mm, d=[0.8, 2.55] mm)

#### III. BEAM STEERING REFLECTARRAY

The unit-cell previously discussed has been adopted for the design of two reflectarrays having the same configuration of the RA depicted in Fig. 1. Both the RAs have been designed with a side  $D = 15.6\lambda_0$ , corresponding to a discretization in 2704 reradiating elements. The aperture is illuminated by a 3D-printed smooth wall horn [47], whose radiation pattern can be modelled as  $cos(\theta)^q$  with q = 12.5. The F distance between the phase center of the feed and the center of the planar aperture is 186 mm ( $F/D \sim 1.2$ ). This value of F was chosen to optimize the illumination taper and the aperture efficiency of the reflectarray. Using this distance, the resulting edges taper is equal to -9.5 dB. The beam-scanning is obtained moving the feed in the vertical plane along a circular arc with radius F. A sketch of the antenna beam-scanning mechanism, with the information on the coordinate reference system, is shown in Fig.4: referring to it, the vertical plane is the yz-plane, where the beam pointing direction  $\theta_{bp}$  changes consequently to the rotation of the feed.

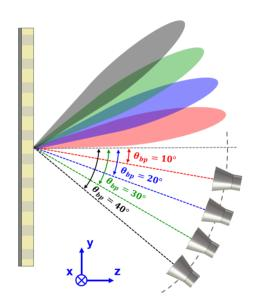


Fig. 4.: Beam-scanning reflectarray meachanism obtained moving the feed in the vertical plane along a circular arc with radius F for different scanning angles.

## A) Single focus RA: design and numerical analysis

In order to check the scanning capabilities of the unit-cell, a first, single focus reflectarray is designed to produce a pencil-beam in the broadside direction when it is center-fed, which corresponds to the beam pointing angles ( $\theta_{bp} = 0^{\circ}, \varphi_{bp} = 0^{\circ}$ ). The required

phase distribution that produces this beam feature is shown in Fig. 5 and can be calculated as follows

$$\phi_R(x_m, y_n) =$$

$$= k_0 (d_{mn} - (x_m \cos(\varphi_{bp}) + y_n \sin(\varphi_{bp})) \sin(\theta_{bp}))$$
(1)

where  $d_{mn}$  is the distance from the phase center of the feed to each cell, while  $(x_m,y_n)$  represent the position of each element in the RA aperture. The design was carried out using only the phase curves obtained in the case of normal incidence. This assumption can be considered reliable due to the favorable behavior of the unit-cell under oblique incidence, seen in the previous sections. The resulting RA is then numerically analyzed with CST Microwave Studio, not considering the position of the feed for which the reflecting surface is designed, but moving the horn along the circular arc of radius F, in such a way that  $\theta_{bp}$  varies between 10° and 40°. A picture of the 3D CAD model of the single focus RA is shown in Fig. 6a. Because of the symmetry of the structure, this corresponds also to cover the range of variation going from  $-40^{\circ}$  to  $-10^{\circ}$ , so that a total scan range given by  $[-40^{\circ}, -10^{\circ}] \cup [10^{\circ}, 40^{\circ}]$  can be achieved. For sake of clearness, just the results related to the positive scanning range  $[10^{\circ}, 40^{\circ}]$  are plotted.

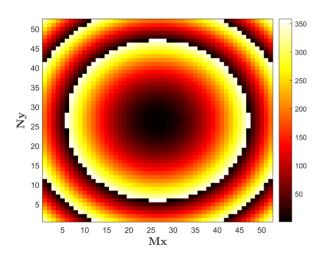


Fig. 5.: Required phase distribution of the  $52 \times 52$  single focus RA.  $M_x$  and  $N_y$  refer to the number of elements in x and y directions, respectively.

The obtained radiation patterns in the vertical (E-) plane and for different pointing directions are plotted in Fig. 7, while the solid line curve in Fig.8 represents the variation of the gain with the pointing direction for this RA. As expected, the radiation patterns and in particular the main beam degrade over the considered scanning range; however, moving the pointing direction from  $\theta_{bp}=10^\circ$  to  $\theta_{bp}=30^\circ$  the gain decreases

by only 1.1 dB. A more important degradation of the radiation performance can be noticed for the pattern pointing to  $\theta_{bp}=40^{\circ}$  characterised by a gain loss of almost 3.5 dB and an enlargement of the main beam.

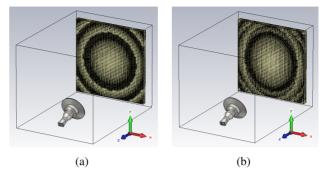


Fig. 6.: 3D CAD model of the two designed dielectric reflectarrays: (a) Single focus; (b) Bifocal.

In Fig. 9, it is shown the effect of the beam-steering on the bandwidth: also in this case, the solid line curve refers to the single focus reflectarray, and it reveals that the 1-dB gain bandwidth is slightly lower than 19% for  $\theta_{bp}=10^\circ$ , while as it can be predicted by the behaviour of the gain, it increases up to 38% for  $\theta_{bp}=40^\circ$ .

The results on both the scanning performance and the bandwidth are promising, and suggest that the proposed unit-cell is a potentially good candidate for designing reflectarrays with scanning-beam capabilities and enhanced bandwidth with respect to other solutions.

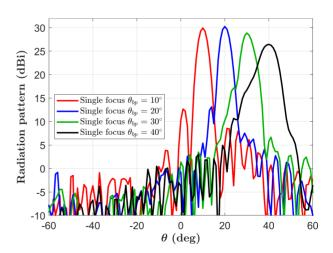


Fig. 7.: Simulated radiation patterns in the vertical plane for four different scanning angles, obtained through the numerical analysis of the single focus reflectarray.

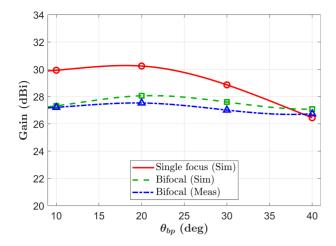


Fig. 8.: Variation of the gain with the pointing direction. Solid line: simulated single focus RA; dashed line: simulated bifocal RA; dash-dotted line: measured bifocal RA.

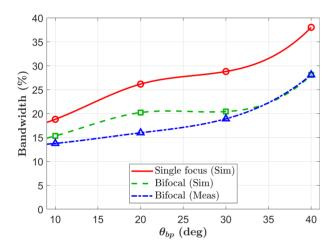


Fig. 9.: Variation of the 1-dB gain bandwidth with the pointing direction. Solid line: simulated single focus RA. Dashed line: simulated bifocal RA. Dash-dotted line: measured bifocal RA.

### B) Bifocal RA: design, manufacturing, numerical and experimental characterization

Since the analysis summarized above confirms the suitability of the UC, it is adopted for the design of a bifocal reflectarray, that is expected to have improved scanning features with respect to the single focus configuration. In order to cover the same scan range considered in Sect.III.A, and taking into account of the structure symmetries, the bifocal RA is designed to provide the phase distribution  $\Phi_{mean}$  shown in Fig. 10 and obtained as:

$$\Phi_{mean} = \frac{\Phi_1 + \Phi_2}{2} \tag{2}$$

where  $\Phi_1$  and  $\Phi_2$  are the phase distributions required to generate a collimated beam pointing to  $\theta_{bp1}=-30^\circ$  and  $\theta_{bp2}=+30^\circ$  respectively. These distributions were obtained using Eq. 1 and using the phase curve related to normal incidence for both focal points.

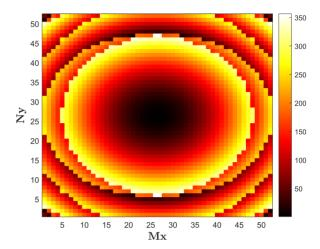


Fig. 10.: Required phase distribution of the  $52\times52$  bifocal RA.  $M_x$  and  $N_y$  refer to the number of elements in x and y directions, respectively.

The designed bifocal reflectarray has been simulated with CST MS and a picture of its 3D CAD model is shown in Fig. 6b. A prototype of the reflectarray was manufactured using the Polyjet based machine Objet30 (provided by Stratasys®) and then experimentally characterized. From the picture in Fig. 11a it appears that, due to the required phase distribution and to the chosen additional reference phase, in the central part of the reflectarray the unit-cells are characterized by smaller values of the holes, that increase going to the edges. This configuration is designed also in view of the results on the dependence from the incidence angle of the UC summarized in Fig. 3 and already discussed. Since the limitations introduced by the adopted 3D printer are taken into account in the UC design, none of smaller holes results to be blocked. The holes set all around the RA surface are added for fixing it to the metallic ground plane through the use of a frame manufactured with FDM 3D printing technique. Fig. 11b shows the entire antenna structure.

In Fig. 12 both the simulated and the measured radiation patterns for different pointing directions at the design frequency are plotted. First, it is worth to note the very good agreement between the numerical and experimental results, confirmed by the performance summarized in Table 1. As expected, the radiation patterns of the bifocal RA are better than those of the single focus configuration, since they are characterized by a more constant gain over the entire scan

Method	Bifocal							
	(Sim)	(Meas)	(Sim)	(Meas)	(Sim)	(Meas)	(Sim)	(Meas)
$\theta_{bp}$ [deg]	±10	±10	±20	±20	±30	±30	±40	±40
Gain [dBi]	27.3	27.2	28.1	27.5	27.6	27.0	27.1	26.7
$\eta_{ap}$	17.6	17.2	20.9	18.5	18.8	16.4	16.7	15.4
1-dB BW [%]	15.3	13.8	20.2	16.0	20.4	18.9	28.1	28.1
HPBW [deg]	6.1	6.5	5.8	5.9	6.2	6.1	6.5	6.9
SLL [dB]	-13.4	-13.8	-12.7	-15.1	-14.5	-15.6	-14.9	-15.3

Table 1. Summary of the simulated and measured bifocal RA performance for different pointing directions.

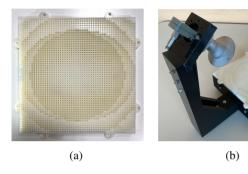


Fig. 11.: 3D-printed dielectric bifocal reflectarray with mechanical beam-steering: (a) Prototype top view; (b) Complete antenna structure.

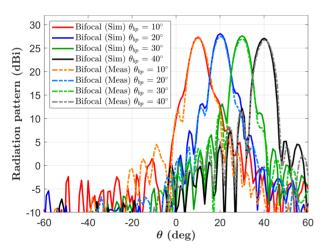


Fig. 12.: Radiation patterns in the vertical plane for four different pointing directions, obtained through the numerical analysis (solid line) and the measurement (dashed line) of the bifocal reflectarray.

range and consequently by a less remarkable enlargement of the beam width. As emerges from Table 1, both the numerical analysis and the measurements of the bifocal RA confirm that the HPBW changes less than 1 degree over the entire scan range, the SLL is always below -13.8 dB and the maximum gain scan loss is about 0.8 dB, as also shown by the dashed and

dot-dashed line curves in Fig. 8, that are almost flat. As expected, the gain slightly reduces for pointing direction closer to broadside, which are farther from those considered for the design of the bifocal surface. Moreover, as typical of a bifocal configuration the maximum gain is lower of almost 2 dB than the one of the single focus configuration, but this is the price to pay for keeping it more constant over the scan range. As expected, the gain reduction entails also a lowering of the aperture efficiency, that for the single focus configuration, when the pointing direction is that for which the antenna is designed, is of the order of 40%.

For what concerns the 1-dB gain bandwidth, from Fig. 9 it appears that it is reduced with respect to that of the single focus configuration. Nevertheless, the results reported in the third row of Table 1 prove that it is slightly lower than 14% for  $\theta_{bp}=10^\circ$  but it increases in the other considered pointing directions. This is a remarkable achievement for a relatively large aperture, since larger structures are generally more challenging to design and analyze, requiring higher levels of accuracy and uniformity. This adds even more significance to the presented results compared to smaller structures typically reported in the literature.

Finally, in Table 2 the measured performance of the bifocal reflectarray is compared with those of other passive scanning beam RAs. Comparing the data relating to their size (row 3) it appears that the here proposed antenna has the largest aperture: this is to take into account discussing its radiating features, since it is well known that properties as the bandwidth decrease with the increasing of the aperture. For what concerns the scan range, only that covered by the RA in [35] is larger than the one considered here. The most remarkable performance of the designed reflectarray is the gain loss  $\Delta G$ , equal to 0.8 dB over the entire scan range, significantly lower than the value obtained in [35] and comparable with the value reported in [37], which however refers to a smaller configuration and a narrower scan range. It is worth to notice that if the extremes of the variation interval for the pointing angle are reduced to  $\pm 30^{\circ}$ ,

as considered in [37, 38], the measured gain scan loss provided by the here presented reflectarray is of the order of 0.2 dB only. The comparison among the maximum achieved 1-dB gain bandwidth confirms the good properties of the dielectric unit-cell: as a matter of fact, the proposed RA and that in [38] have a band that is significantly wider than the other two reported structures.

**Table 2.** Comparison between the measured features of proposed passive bifocal beam-scanning RA and those of other similar configurations available in the literature.

Ref.	[37]	[35]	[38]	This work
Freq. [GHz]	32	12	30	30
Aperture $[\lambda_0^2]$	227	64	129.3	243.36
F/D	0.725	1	2	1.2
Design	bifocal	PMM	bifocal	bifocal
Dielectric	N	N	Y	Y
Scan range	±30°	±45°	±30°	±40°
Max 1-dB gain BW [%]	4.3	10	25.4	28
ΔG [dB]	0.75	1.95	1.1	0.8
SLL [dB] at 30°	-12	-15	-18.4	-15.6

#### IV. CONCLUSIONS

In this paper, a dielectric unit-cell is used to design a reflectarray with favorable beam-steering capabilities and enhanced bandwidth. After having checked the performance of the UC, a bifocal reflectarray has been designed, manufactured with a 3D printer and experimentally characterized. The results confirms the RA good scanning capabilities, characterized by gain losses of the order of 0.8 dB over a  $\pm 40^{\circ}$  scan range, while the measured 1-dB bandwidth is attested to vary from 13% up to 28% over the entire scanning region. These results demonstrate the capability of 3D-printing technology for producing high-performance, cost-effective reflectarray antennas with wideband behavior and excellent beamsteering capabilities. Moreover, the proposed bifocal approach applied to a dielectric-only RA highlights the potential for a wide range of practical applications, from radars to wireless networking. A further improvement of this feature can be obtained adopting a proper optimization technique, like that used in [42], for the design of a beam-scanning reflectarray.

#### REFERENCES

- J. Huang and J. Encinar, Reflectarray antennas. Wiley-IEEE press, 2008.
- [2] P. Nayeri, F. Yang, and A. Z. Esherbeni, Reflectarray antennas: theory, designs and applications, Hoboken, NJ, USA: Wiley, 2018.
- [3] J.A. Encinar, "Design of two-layer printed reflectarray using patches of variable size," IEEE Trans. Antennas Propag., vol. 49, no. 10, pp. 1403-1410, 2001
- [4] J.A. Encinar and J.A.Zornoza, "Broadband design of three-layer printed reflectarrays," IEEE Trans. Antennas Propag., vol. 51, no. 7, pp. 1662-1664, 2003.
- [5] M.R. Chaharmir, J. Shaker and H. Legay, "Broadband design of a single layer large reflectarray using multi cross loop elements," IEEE Trans. Antennas Propag., vol. 57, no. 10, pp. 3363-3366, 2009.
- [6] J.H. Yoon, Y.J. Yoon, W.-S. Lee and J.-H. So, "Broadband microstrip reflectarray with five parallel dipole elements," IEEE Antennas Wireless Propag. Lett., vol. 14, pp. 1109-1112, 2015.
- [7] Q. Wang, Z.H. Shao, Y.J. Cheng and P.K. Li, "Broadband low-cost reflectarray using modified double-square loop loaded by spiral stubs," IEEE Trans. Antennas Propag., vol. 63, no. 9, pp. 4224-4229, 2015.
- [8] X. Li, X. Li, Y. Luo, G. Wei and X. Yi, "A Novel Single Layer Wideband Reflectarray Design Using Two Degrees of Freedom Elements," IEEE Trans. Antennas Propag., vol. 69, no. 8, pp. 5095-5099, 2021.
- [9] D. Kundu, D. Bhattacharya and R. Ruchi, "A Single-Layer Broad-band Reflectarray in K-Band Using Cross-Loop Slotted Patch Elements," IEEE Access, vol. 10, pp. 13490-13495, 2022.
- [10] S. Zhang, "Three-dimensional printed millimetre wave dielectric resonator reflectarray," IET Microw. Antennas Propag., vol. 11, no. 14, pp. 2005-2009, 2017.
- [11] M.D. Wu et al., "Design and Measurement of a 220 GHz Wideband 3-D Printed Dielectric Reflectarray," IEEE Antennas Wireless Propag. Lett., vol. 17, no. 11, pp. 2094-2098, 2018.
- [12] X. Zhao, F. Wei, B. Li and X. Shi, "Design of circularly polarized dielectric resonator reflectarray antenna," Proc. Asia-Pacific Microw. Conf. (APMC), 2018, pp. 1552-1554.
- [13] P. Mei, S. Zhang and G. F. Pedersen, "A Wideband 3-D Printed Reflectarray Antenna With Mechanically Reconfigurable Polarization," IEEE Antennas Wireless Propag. Lett., vol. 19, no. 10, pp. 1798-1802, 2020.
- [14] B. Li, C. Y. Mei, Y. Zhou and X. Lv, "A 3-D-Printed Wideband Circularly Polarized Dielectric Reflectarray of Cross-Shaped Element," IEEE Antennas Wireless Propag. Lett., vol. 19, no. 10, pp. 1734-1738, 2020.
- [15] Y. Cui, S. A. Nauroze, R. Bahr and E. M. Tentzeris, "3d printed one-shot deployable flexible 'Kirigami' dielectric reflectarray antenna for mm-wave applications," IEEE MTT-S Int. Microw. Symp. Dig., 2020, pp. 1164-1167.
- [16] Q. Cheng et al., "Dual Circularly Polarized 3-D Printed Broadband Dielectric Reflectarray With a Linearly Polarized Feed," IEEE Trans. Antennas Propag., vol. 70, no. 7, pp. 5393-5403, 2022.
- [17] H. Yu, P. Li, J. Su, Z. Li, S. Xu and F. Yang, "Reconfigurable Bidirectional Beam-Steering Aperture with Transmitarray, Reflectarray, and Transmit-Reflect-Array Modes Switching," IEEE Trans. Antennas Propag., 2022.
- [18] B. J. Xiang, X. Dai and K. -M. Luk, "A Wideband Low-Cost Reconfigurable Reflectarray Antenna With 1-Bit Resolution," IEEE Trans. Antennas Propag., vol. 70, no. 9, pp. 7439-7447, 2022.

- [19] S. -G. Lee, Y. -H. Nam, Y. Kim, J. Kim and J. -H. Lee, "A Wide-Angle and High-Efficiency Reconfigurable Reflectarray Antenna Based on a Miniaturized Radiating Element," IEEE Access, vol. 10, pp. 103223-103229, 2022.
- [20] N. Zhang et al., "A Dual-Polarized Reconfigurable Reflectarray Antenna Based on Dual-Channel Programmable Metasurface," IEEE Trans. Antennas Propag., vol. 70, no. 9, pp. 7403-7412, 2022.
- [21] B. Xi, Y. Xiao, K. Zhu, Y. Liu, H. Sun and Z. Chen, "1-Bit Wideband Reconfigurable Reflectarray Design in Ku-Band," IEEE Access, vol. 10, pp. 4340-4348, 2022.
- [22] F. Wu, R. Lu, J. Wang, Z. H. Jiang, W. Hong and K. -M. Luk, "Circularly Polarized One-Bit Reconfigurable ME-Dipole Reflectarray at X-Band," IEEE Antennas Wireless Propag. Lett., vol. 21, no. 3, pp. 496-500, 2022.
- [23] H. Li, X. Qi, T. Zhou, Z. Xu and T. A. Denidni, "Wideband Reconfigurable Reflectarray based on Reflector-backed Second-order Bandpass Frequency Selective Surface," IEEE Trans. Antennas Propag., 2022
- [24] S. -G. Zhou et al., "A Wideband 1-Bit Reconfigurable Reflectarray Antenna at Ku-Band," IEEE Antennas Wireless Propag. Lett., vol. 21, no. 3, pp. 566-570, 2022.
- [25] J.-M. Baracco, P. Ratajczak, P. Brachat, J.-M. Fargeas and G. Toso, "Ka-Band Reconfigurable Reflectarrays Using Varactor Technology for Space Applications: A proposed design," IEEE Antennas Propag. Mag., vol. 64, no. 1, pp. 27-38, 2022.
- [26] I. -J. Nam, S. Lee and D. Kim, "Miniaturized Beam Reconfigurable Reflectarray Antenna With Wide 3-D Beam Coverage," IEEE Trans. Antennas Propag., vol. 70, no. 4, pp. 2613-2622, 2022.
- [27] X. Liu et al., "Terahertz Beam Steering Using a MEMS-Based Reflectarray Configured by a Genetic Algorithm," IEEE Access, vol. 10, pp. 84458-84472, 2022.
- [28] H. Kim, J. Kim and J. Oh, "A Novel Systematic Design of High-Aperture-Efficiency 2D Beam-Scanning Liquid-Crystal Embedded Reflectarray Antenna for 6G FR3 and Radar Applications," IEEE Trans. Antennas Propag. vol. 70, no. 11, pp. 11194-11198, 2022.
- [29] X. Li, H. Sato, Y. Shibata, T. Ishinabe, H. Fujikake and Q. Chen, "Development of Beam Steerable Reflectarray With Liquid Crystal for Both E-Plane and H-Plane," IEEE Access, vol. 10, pp. 26177-26185, 2022.
- [30] W. Zhang, Y. Li and Z. Zhang, "A Reconfigurable Reflectarray Antenna With an 8  $\mu$ m-Thick Layer of Liquid Crystal," IEEE Trans. Antennas Propag., vol. 70, no. 4, pp. 2770-2778, 2022.
- [31] E. Carrasco, J. Gomez-Cruz, M. Serrano-Berrueco, C. E. Saavedra and C. Escobedo, "Design of Microfluidic Reflectarray Elements for Multi-Reconfiguration Using Liquid Metal," IEEE Open Jou. Antennas Propag., vol. 3, pp. 425-434, 2022.
- [32] H. Zhang, W. Wu, Q. Cheng, Q. Chen, Y. -H. Yu and D. -G. Fang, "Reconfigurable Reflectarray Antenna Based on Hyperuniform Disordered Distribution," IEEE Trans. Antennas Propag., vol. 70, no. 9, pp. 7513-7523, 2022.
- [33] A. J. Rubio, A. -S. Kaddour and S. V. Georgakopoulos, "A Mechanically Rollable Reflectarray With Beam-Scanning Capabilities," IEEE Open Jou. Antennas Propag., vol. 3, pp. 1180-1190, 2022.
- [34] P. Nayeri, F. Yang and A. Z. Elsherbeni, "Beam-Scanning Reflectarray Antennas: A Technical Overview and State of the Art," IEEE Antennas Propag. Mag., vol. 57, no. 4, pp. 32-47, 2015.
- [35] G.-B. Wu, S.-W. Qu and S. Yang, "Wide-Angle Beam-Scanning Reflectarray With Mechanical Steering," IEEE Trans. Antennas Propag., vol. 66, no.1, pp. 172-181, 2018.

- [36] P. Mei, S. Zhang, and G. F. Pedersen, "A Low-Cost, High-Efficiency and Full-Metal Reflectarray Antenna With Mechanically 2-D Beam-Steerable Capabilities for 5G Applications," IEEE Trans. Antennas Propag., vol. 68, no. 10, pp. 6997-7006, 2020.
- [37] P. Nayeri, F. Yang and A. Z. Elsherbeni, "Bifocal Design and Aperture Phase Optimizations of Reflectarray Antennas for Wide-Angle Beam Scanning Performance," IEEE Trans. Antennas Propag., vol. 61, no. 9, pp. 4588-4597, 2013.
- [38] Y. Cui, R. Bahr, S. A. Nauroze, T. Cheng, T. S. Almoneef and M. M. Tentzeris, "3D Printed 'Kirigami'-Inspired Deployable Bi-Focal Beam-Scanning Dielectric Reflectarray Antenna for mm-Wave Applications," IEEE Trans. Antennas Propag., vol. 70, no. 9, pp. 7683-7690, 2022.
- [39] P. Pirinoli, T. Lohrey, M. Orefice, M. Beccaria and G. Dassano, "Multifocal Approach for Reflectarray Antenna for DTH Applications," 15th Eur. Conf. on Antennas Propag. (EuCAP), 2021, pp. 1-4.
- [40] P. Pirinoli, T. Lohrey, M. Orefice, M. Beccaria and G. Dassano, "Reflectarray with mechanically steerable beam for DTH application," 49th Eur. Microw. Conf. (EuMC), 2019, pp. 141-144.
- [41] G.-B. Wu, S. -W. Qu, S. Yang and C. H. Chan, "Low-Cost 1-D Beam-Steering Reflectarray With ±70° Scan Coverage," IEEE Trans. Antennas Propag., vol. 68, no. 6, pp. 5009-5014, 2020.
- [42] A. Niccolai, M. Beccaria, R. E. Zich, A. Massaccesi and P. Pirinoli, "Social Network Optimization Based Procedure for Beam-Scanning Reflectarray Antenna Design," IEEE Open Jou. of Antennas Propag., vol. 1, pp. 500-512, 2020.
- [43] A. Massaccesi, M. Beccaria and P. Pirinoli, "3D-printable Perforated Dielectric Reflectarray in Ka-band," 2019 IEEE Int. Symp. on Antennas Propag., 2019, pp. 295-296.
- [44] A. Massaccesi, M. Beccaria and P. Pirinoli, "Beam Steering mm-Waves Dielectric-only Reflectarray," 2022 Microw. Medi. Symp. (MMS), 2022, pp. 1-4.
- [45] A. Massaccesi, et al., "3D-Printable dielectric transmitarray with enhanced bandiwidth at millimiter-waves," IEEE Access, vol. 6, pp. 46407-46418, 2018.
- [46] A. Massaccesi, G. Dassano, and P. Pirinoli, "Beam scanning capabilities of a 3D-printed perforated dielectric transmitarray", Electronics, vol. 8, no. 4, 2019.
- [47] Beccaria M, Addamo G, Orefice M, Peverini O, Manfredi D, Calignano F, Virone G and P. Pirinoli, "Enhanced Efficiency and Reduced Side Lobe Level Convex Conformal Reflectarray," Applied Sciences, vol. 11, no. 21, 2021.

#### **AUTHOR BIOGRAPHIES**



Andrea Massaccesi was born in Osimo, Italy, in 1987. He received the B.S. degree in electronic engineering from the Università Politecnica delle Marche, Ancona, Italy, in 2012, the M.S. degree in electronic engineering and the Ph.D. degree (cum laude) in electrical, electronic and communication engineering from the Politecnico di Torino, Turin, Italy, in 2015 and 2019, respectively. From November 2017 to May 2018, he was a visiting Ph.D. student with Loughborough

University, Loughborough, U.K., within the Symeta research program. Since January 2020, he has been a Research Fellow with the Department of Electronics and Telecommunications, Politecnico di Torino, Turin, Italy. His research activities include the study of underwater electromagnetic propagation and the design of proper antennas for underwater environments, the design and manufacturing of transmitarray and reflectarray antennas exploiting 3D-printing techniques, and the development

of efficient global optimization techniques suitable for electromagnetic problems.

microsensors for industrial applications, on the development of microfluidics and lab-on-a-chip for biomedical applications and, more recently, on the development and application of 3-D printing polymeric technologies.



Michele Beccaria was born in Enna, Italy, on July 24, 1991. He received the B.Sc, the M.Sc. degree, and the Ph.D. degree (cum laude) in applied electromagnetics from the Politecnico di Torino in 2013, 2015, and 2019, respectively. He has been a Research Fellow with the Department of Electronics and Telecommunications, Politecnico di Torino, Turin, since January 2019, and has been an Assistant Professor since 2023. In 2017 and 2018, he was a visiting Ph.D. student

with Tsinghua University, Beijing, China, under the supervision of Prof. Fan Yang. His research interests include reflectarray antennas, transmitarray antennas, smart electromagnetic surfaces and the application of new optimization algorithms for complex antenna design. He was also recognized as the winner of two grants for attending the Ph.D. courses of ESoA in 2016 and in 2018 as one of the Best Ph.D. Students at Politecnico di Torino with the Ph.D. Quality Award. He was included in the Technical Committee of Conference of International Relevance (ICCE 2018, 2020) and serves many journals of the IET group as a reviewer. In 2020, he received the 2019 IEEE AP/ED/MTT North Italy Chapter Thesis Awards with the Best Ph.D. Thesis Antennas and Propagation Society for the thesis "Design of Innovative Reflectarray and Transmitarray Antennas."



Valentina Bertana received her BSc and MSc Degree in Biomedical Engineering at Politecnico di Torino in 2013 and 2015 respectively. In February 2020 she received her PhD degree at Politecnico di Torino in Electrical, Electronic and Communication Engineering. Her research activities are mainly focused on additive manufacturing, smart materials, printable electronics and microfluidics.



Simone Luigi Marasso received his Master degree in Biomedical Engineer and Ph.D. degree in Electronic Devices from Politecnico di Torino, Turin, Italy, in 2005 and 2010, respectively. From 2005 to 2011, he had a fellowship with Politecnico di Torino, Turin, Italy and he worked at Chilab, materials and microsystem labratory at Chivasso, Italy. Since 2014 he is a CNR researcher, IMEM, @ Politecnico di Torino DISAT department. His research activities focus

on design and fabrication of MEMS, Lab on Chip and microfluidic devices as demonstrated by his scientific publications in these fields.



Matteo Cocuzza obtained the degree in Electronic Engineering at the Polytechnic of Turin in 1997 and the PhD in Electronic Devices in 2003. He is currently Associate Professor at the Department of Applied Science and Technology of the Polytechnic of Turin and associate researcher of IMEM-CNR. In 1998 he was one of the founders of the Chilab-Materials and Microsystems Laboratory and recently co-founder of the new technological facility PiQuET – Piedmont Quantum

Enabling Technologies. He is currently lecturer of master's degree courses in the field of micro and nanotechnologies, microsensors, MEMS, also in the context of the international Master in Nanotechnology for ICT (joint master between Politecnico di Torino, INPG Grenoble and EPFL Lausanne). His research activity is focused on the development of MEMS and



Gianluca Dassano received the Laurea degree in electronic engineering from the Politecnico di Torino, Italy, in 1999. Since 1999, he has been with the Department of Electronics and Telecommunications, Politecnico di Torino, as a Technician with the Electromagnetic Group, with particular interest in antenna application. At present, his main activities concern antenna prototyping and characterization inside the Laboratory of Antennas and EMC.



Paola Pirinoli received the M.S. (Laurea) and Ph.D. (Dottorato di Ricerca) degrees in electronic engineering from the Politecnico di Torino, Italy, in 1989 and 1993, respectively. From 1994 to 2003, she was an Assistant Professor (Ricercatore) of electromagnetic fields with the Department of Electronics and Telecommunications, Politecnico di Torino, where she was an Associate Professor from 2003 to 2018, and has been a Full Professor since 2018. From 1996

to 1997, she was a Visiting Research Fellow with the University of Nice, Sophia Antipolis, France. In 2014, 2015, and 2017, she was a Visiting Research Fellow with Tsinghua University, Beijing, China. She has coauthored around 250 journal articles and conference papers. Her main research activities include the development of analytically based numerical techniques, essentially devoted to the fast and accurate analysis of printed structures on planar or curved substrates, the modeling of nonconventional substrates, as chiral and anisotropic ones, the development of innovative and efficient global optimization techniques, and the design of innovative reflectarray and transmitarray antennas. In 1998, she received the URSI Young Scientist Award and the Barzilai Prize for the Best Paper at the National Italian Congress of Electromagnetic (XII RiNEm). In 2000, she was the recipient of the Prize for the Best Oral Paper on Antennas at the Millennium Conference on Antennas and Propagation. She serves as a reviewer for several international journals and conferences. She is a member of the TPC and the organizing committee of several international conferences.